AUT Journal of Electrical Engineering

AUT J. Elec. Eng., 58(1) (2026) 45-58
DOI: 10.22060/eej.2025.24305.5677

Efficient Control and Five-Level MMC Integration for Power Quality Improvement in DFIG-Based Wind Energy System

Kunche Gowthami[1]*, Dondapati Ravi Kishore[2], Inti Sai Deepthi[1], Kolapati Durga Prasad[1], Gandham Satish Kumar[1]

[1] Department of Electrical and Electronics Engineering, Godavari Institute of Engineering and Technology, Rajahmundry, India.
[2] Department of Electrical and Electronics Engineering, Godavari Global University, Rajahmundry, India.

ABSTRACT: The main objectives of the study are to address Power Quality (PQ) problems caused by shifting load demands, including voltage instability and harmonic distortion, which affect system performance and reduce stability. To achieve the set goals, the following tasks were accomplished: the design and implementation of a 5-Level Modular Multilevel Converter (MMC) powered by a Double Fed Induction Generator (DFIG)-based wind system, the application of advanced control techniques utilizing D-Q theory and a Hysteresis Current Controller (HCC) for stable current injection, and the incorporation of an LC filter to enhance AC supply quality. The most important results are the reduction of total harmonic distortion (THD) to 1.35%, enhanced voltage stability, and improved overall PQ, validated through MATLAB simulations. The significance of the obtained results is the development of a robust and efficient system that addresses PQ issues, offering a substantial improvement over state-of-the-art methods and ensuring high-quality power delivery to the grid.

Review History:

Received: Jun. 21, 2025
Revised: Sep. 03, 2025
Accepted: Oct. 18, 2025
Available Online: Jan. 10, 2026

Keywords:

Power Quality (PQ)
5-Level MMC
DFIG-Wind System
DQ- Sheory
HCC

1- Introduction

The growth in production of energy using renewable technologies is largely driven by addressing environmental issues, specifically global warming [1]. Governments and Organizations are promoting clean energy, with wind source playing a crucial role owing to its minimal environmental impact. In wind systems, DFIGs [2] are extensively utilized for their ability to perform efficiently at a wide range of wind conditions. The DFIG-assisted Wind Energy Conversion System (WECS) configuration allows for independent regulation of active and reactive power, making it ideal for integration. Nevertheless, WECS faces power quality problems, including voltage stability, imbalanced reactive power, and harmonic distortions [3]. The inherent variability of wind and the switching operation of power electronic devices poses challenge in grid compatibility.

As time progressed, a wide array of converter topologies has been designed by researchers to resolve these challenges. The Voltage Source Converter (VSC) of literature [4] is a simple topology that switches the DC link voltage between positive and negative levels. In addition, significant losses occur, which affect the system efficiency, making it less suitable for power applications [5]. As a consequence, multilevel inverter and converter topologies have been developed. The 3-Level Neutral Point Clamped (NPC) [6, 7] converter is introduced as an improvement over VSC, minimizing harmonics with the generation of 3-Level output, but complexity arises in balancing neutral point voltage. Another advancement presented in Reference [8, 9] is the flying capacitor multilevel converter, which improves the performance by utilizing capacitors and storage elements for the generation of multiple voltage steps. This allows for improved reduction in harmonics and offers redundancy, enhancing the reliability of the system. However, this requires a larger number of capacitors, which increases the system size, and also suffers from complex control and higher losses in capacitors. Overwhelming the limitations, the Cascaded H-Bridge inverter[10] has emerged as a potential solution for high power applications, owing to its modular structure and excellent performance towards the mitigation of harmonics. This topology included multiple H-bridge inverters [11, 12] attached in series, powered using a DC source, allowing for nearly sinusoidal output. The design model of the CHB converter [13] is highly scalable and fault-tolerant, owing to its operation even under the isolation of individual modules, but it requires multiple DC sources. Still, the CHB converter marks a significant leap forward in dealing with power quality issues in wind energy systems. The limitations of these earlier topologies, particularly in terms of harmonic distortion, scalability, and efficiency, paved the way for the development of MMC [14].

MMC technology brings benefits, including reduced

*Corresponding author's email: gowthami75.k@gmail.com

harmonic distortion and enhanced system efficiency through its modular design. Nevertheless, the generation of reference current is essential to align with the output current and the reference value. In Reference [15], Instantaneous Reactive Power Theory (IRPT) is presented, which generates reference signals with an offset value to zero at cut-off frequencies, but struggles with dynamic responses. Another technique presented in [16] is Short-Time Fourier Transform (SIFT) for the generation of reference current, where the signal is segmented for applying the Fourier Transform. However, the approach requires significant resource computation, posing limitations for real-time applications that demand quick response and processing efficiency. In Reference [17], a harmonic current estimation technique based on the trigonometric orthogonal principle is presented. While effective, it is characterized by high computational demand and slower processing speeds.

In response to the limitations identified, the proposed work contributes several improvements, such as,

Implementation of 5-Level MMC for efficient conversion of voltage and better suppression of harmonics, resulting in cleaner output.

Utilizes DFIG-based wind source, ensuring system stability with stabilized DC link voltage for the MMC system, improving power quality.

Introduction of HCC, ensuring that the actual current closely matches the desired reference, thus maintaining power quality.

A combination of DQ theory and MMC effectively reduces the harmonics and supports in handling non-linear loads.

The proposed combination of a 5-Level MMC powered by a DFIG-based wind system, advanced D-Q theory with HCC control, and an LC filter is superior to existing methods because it integrates the strengths of multiple advanced techniques to comprehensively address power quality issues. While traditional converters often suffer from higher switching losses, limited voltage levels, and higher harmonic distortion, the 5-Level MMC generates smoother stepped waveforms with reduced harmonics. The use of D-Q theory with HCC ensures precise and dynamic current control, enabling rapid compensation of disturbances and maintaining voltage stability even under fluctuating load conditions. Additionally, the LC filterfurther suppresses residual harmonics, ensuring near-ideal sinusoidal output. Together, these elements reduce THD while also improving stability and reliability.

The rest of the paper is organized by Section II detailing the description of proposed work, Section III modelling of the system, Section IV Results and Discussion, and the work ged concluded in Section V.

2- Description of Work

The block diagram presented in Fig. 1 illustrates a DFIG-assisted wind energy system employing a 5-Level MMC for improving power quality. The system connects an 3ϕ AC source at the Point of Common Coupling (PCC), where

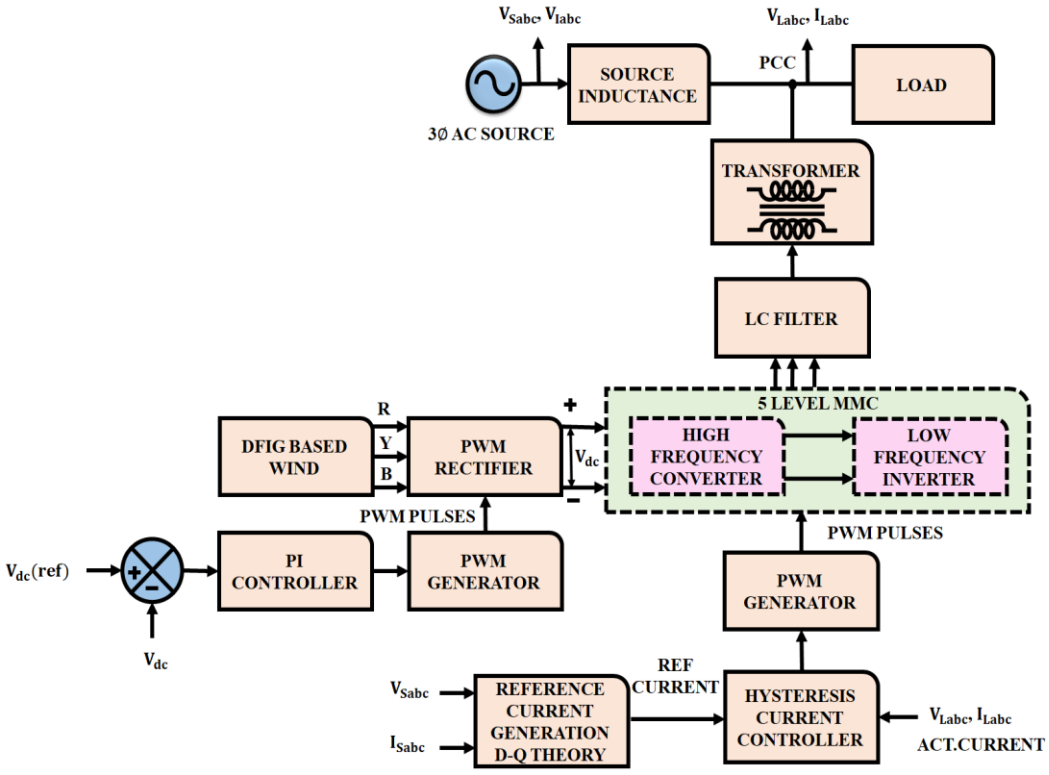

Fig. 1. Proposed MMC Architecture for Power Quality Improvement.

it supplies power to the load. In between, there is source inductance to smooth the connection between the source and load. However, PQ issues arise owing to changes in load. The DFIG system is employed to generate power from wind, which is then converted into DC utilizing a PWM rectifier. The PI controller effectively regulates the DC link voltage by comparing V_{dc} with $V_{dc(ref)}$. Therefore, a stabilized DC link voltage is achieved, which is used for the operation of the 5-Level MMC.

In the 5-Level MMC, the high-frequency converter is responsible for providing high-quality DC output. It is followed by low frequency inverter, which is responsible for the conversion of high-frequency DC into AC that is synchronized with the grid frequency. The inverted output is fed to the LC filter, which assists in the removal of switching harmonics generated by the MMC. The control system uses DQ theory for the generation of reference current, that are aligned with the desired voltage and current parameters. This supports the injection of stabilized and balanced power into the grid and prevents power quality issues. The HCC employed ensures that the actual current matches the reference current generated by DQ theory. As a consequence, the system effectively mitigates power quality issues, including voltage sags, swells, harmonic distortion, and current imbalances, leading to overall improvement in power quality.

3- Modelling of Proposed System

3- 1- Level Modular Multilevel Converter

The 5-Level MMC is a modular and scalable topology, which is capable of generating multiple levels of voltage by controlling a series of submodules (SMs) in each phase. The MMC topology allows for effective conversion of power between AC and DC with minimized losses and harmonic distortions. The topology of the 5-Level MMC is illustrated in Fig. 2. The 5-Level MMC is built using multiple submodules connected in series within each converter arm, which allows it to generate a stepped voltage waveform with five distinct levels. Each submodule typically consists of a capacitor and switching devices, enabling precise control of voltage and current. By appropriately switching these submodules on or off, the MMC synthesizes a staircase-like output voltage that closely approximates a sinusoidal waveform, thereby reducing harmonic distortion and minimizing the need for bulky filters.

The switching table of the 5-level MMC is listed in Table 1, explaining the performance of submodules in each arm in the generation of the desired output. Each arm contains multiple SMs, and in the instance of 5-level MMC, two SMs are in each arm. These SMs contribute the stored capacitor voltage to the output at the switch ON state or are bypassed when the switch is OFF.

In the 5-Level MMC, the switching states of SMs in the upper and lower arms define the output voltage level. Each of the SMs can be either switched ON or OFF by appropriately controlling the SMs in both arms. The switching combination for the generation of voltage levels is as follows:

- **Maximum Positive Voltage:** The upper arms SM_1, SM_2 are in the ON state and the lower arm SM_3, SM_4 are in the OFF state. At this instance, each SMs adds its capacitor voltage, contributing to the total arm voltage. Since SM_3, SM_4 are OFF, there is no contribution of voltage. The overall DC voltage from SM_1, SM_2 is applied across the output terminals, resulting in a maximum voltage of $+V_{dc}/2$.
- **Mid-Level Positive Voltage:** In this case, only one SM in the upper arm contributes its voltage, and there is no voltage from the lower arm. As a consequence, the output voltage is half of the maximum positive voltage, which is $+V_{dc}/4$. This level is suitable for generating smoother transitions in the output waveform and for harmonic reduction.
- **Zero Output Voltage:** When one SM in the upper arm and lower arm are turned ON, the voltage from the upper and lower arm cancels each other. The voltage from the upper arm $+V_{dc}/4$ and from the lower arm $-V_{dc}/4$, results in a net output of zero volts. This balanced switching state creates a neutral or zero-voltage point in the waveform.
- **Mid-Level Negative Voltage:** Here, both SM_1, SM_2 are bypassed, with no voltage support. On SM in lower arm is turned ON, and the capacitor voltage produces a negative voltage of $-V_{dc}/4$, resulting in mid-level negative output voltage.
- **Maximum Negative Voltage:** In this case, the upper arm SM_1, SM_2 is in OFF and the lower arm SM_3, SM_4 is turned ON. The ON state of the lower arm contributes the full capacitor voltage to the output. The upper arm

Table 1. Switching Operation of 5-Level MMC.

SM1 (Upper Arm)	SM2 (Upper Arm)	SM3 (Lower Arm)	SM4 (Lower Arm)	V_{out} (Output Voltage)
1	1	0	0	$+V_{dc}/2$
1	0	0	0	$+V_{dc}/4$
1	0	1	0	0
0	0	1	0	$-V_{dc}/4$
0	0	1	0	$-V_{dc}/2$

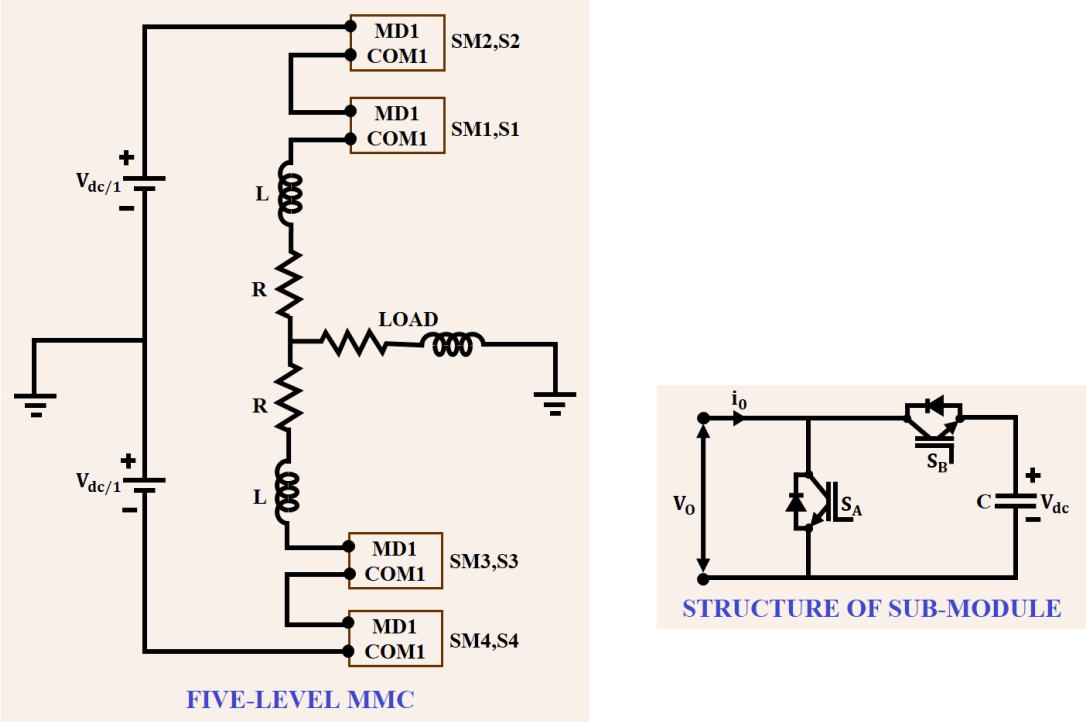

Fig. 2. Five-Level MMC System.

SM_1, SM_2 is bypassed, so there is no voltage contribution. As a consequence, the voltage from the lower arm generates the maximum negative voltage $-V_{dc}/2$.

This combination of switching states allows the MMC to produce a stepped waveform with 5 distinct voltage levels $+V_{dc}/2, +V_{dc}/4, 0, -V_{dc}/4, -V_{dc}/2$. By alternating between these levels, the MMC produces more sinusoidal AC output, with improved power quality, reduced harmonics, and reduces the need for large filters. The switching states are controlled, allowing MMC to generate smoother output and making it ideal for high-power applications.

3- 2- DFIG Driven WECS

In this work, to power the MMC, the DFIG-based WECS is adopted, as shown in Fig. 3, owing to its performance towards varying wind speeds. The wind turbine is accountable for capturing kinetic energy and converting it into mechanical energy. The generated AC output is first processed by a PWM rectifier, which converts it into a regulated DC voltage. This DC link is then fed into an MMC, which produces a high-quality stepped AC output with reduced harmonics for grid integration. To maintain a stable DC voltage, a PI controller continuously compares the actual DC voltage with the reference value and adjusts control signals accordingly. The generated power from a wind turbine is expressed as,

$$P_a = \frac{1}{2}\rho S C_p(\lambda,\beta) V^3 \tag{1}$$

Where the area circled by the wind turbine is noted a S, air density as ρ, wind speed is signified as V and power conversion efficiency as C_p. The aerodynamic torque expression is given by

$$T_a = \frac{P_a}{\Omega_t} = \frac{1}{2\Omega_t}\rho S C_p(\lambda,\beta) V^3 \tag{2}$$

Here, turbine speed is indicated by Ω_t. The DFIG is a wound rotor induction generator that contributes in generation of power.

The voltage expression for DFIG in dq frame is expressed as

$$\begin{cases} V_{ds} = R_s I_{ds} + \dfrac{d}{dt}\varphi_{ds} - \omega_s \varphi_{qs} \\ V_{qs} = R_s I_{qs} + \dfrac{d}{dt}\varphi_{qs} + \omega_s \varphi_{ds} \\ V_{dr} = R_r I_{ds} + \dfrac{d}{dt}\varphi_{dr} - (\omega_s - \omega_r)\varphi_{qs} \\ V_{qr} = R_r I_{qs} + \dfrac{d}{dt}\varphi_{qr} - (\omega_s - \omega_r)\varphi_{ds} \end{cases} \tag{3}$$

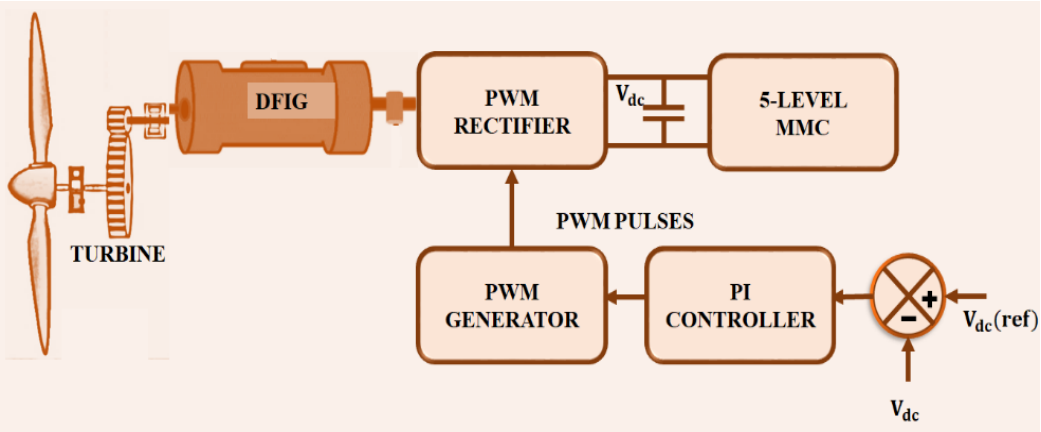

Fig. 3. Architecture of DFIG Driven WECS.

$$\begin{cases} \varphi_{ds} = L_s I_{ds} + M I_{dr} \\ \varphi_{qs} = L_s I_{qs} + M I_{qr} \\ \varphi_{dr} = L_r I_{dr} + M I_{ds} \\ \varphi_{qr} = L_r I_{qr} + M I_{qs} \end{cases} \quad (4)$$

Where rotor and stator indices are represented as r and s , resistance is denoted by R , flux as, synchronous reference frame as d and q . In addition, the electrical frequency is signified a ω s, with V and I expressing voltage and current. The inductance is related as L and mutual inductance as M. The governing mechanical expression for DFIG is stated as

$$J\frac{d\Omega}{dt} = T_a - T_{em} - f\Omega \quad (5)$$

Where the speed of DFIG is indicated as Ω , the total inertia of the turbine as J , damping coefficient as f and electromagnetic torque as T_{em} expressed by

$$T_{em} = p\frac{M}{L_s}\left(\phi_{qs} I_{dr} - \phi_{ds} I_{qr}\right) \quad (6)$$

Here number of pole pairs is written by p . The expression indicating active and reactive power at the stator side is expressed by,

$$\begin{cases} P_s = \frac{3}{2}\left(V_{ds} I_{ds} + V_{qs} I_{qs}\right) \\ Q_s = \frac{3}{2}\left(V_{qs} I_{ds} - V_{ds} I_{qs}\right) \end{cases} \quad (7)$$

The integration of DFIG-WECS with MMC necessitates a controller to manage complex interactions within the system. In this work PI controller is utilized for optimizing the flow of power, maintaining the stability of voltage, and ensuring the efficiency and reliability of the wind system.

3- 3- Hysteresis Current Control

HCC in Fig. 4 is a commonly utilized nonlinear control strategy in power systems for the control of the inverter. The HCC is the hysteresis bandwidth, defining the range within which the current is allowed to vary. The controller operated by maintaining the actual current within the predefined bandwidth around the reference current. The HCC technique continuously compares the actual i_{actual} and reference current i_{ref} and generates an error Δi_e . If the actual current exceeds the upper or lower limits of this band, the inverter switches states to correct it. A narrower bandwidth results in higher current tracking accuracy but increases switching frequency, leading to more switching losses and Electromagnetic Interference (EMI). In contrast, a wider bandwidth lowers switching frequency and losses but reduces current tracking accuracy.

This eliminates the effect on tracking performance compared to triangular wave comparison and does not necessitate a fixed triangular carrier. Initially, the instantaneous deviation (Δi_c) is evaluated by taking the difference between the actual current (i_c) from the compensation current command signal (i_c^*). This deviation is then fed into a hysteresis comparator, where the bandwidth is set to $(2\Delta i_c)$. The actual current is controlled within the range of $i_c^* + \Delta i_c$ and $i_c^* - \Delta i_c$ to follow the command current closely. In case the hysteresis band is too wide, the switching frequency of the inverter decreases, causing low switching losses. However, this also ranks with a larger tracking error, initiating the compensation current to contain more high-frequency harmonics. Conversely, a narrow hysteresis bandwidth improves the tracking accuracy but increases switching frequency, resulting in higher switching losses. Therefore, the switching frequency range is chosen as a

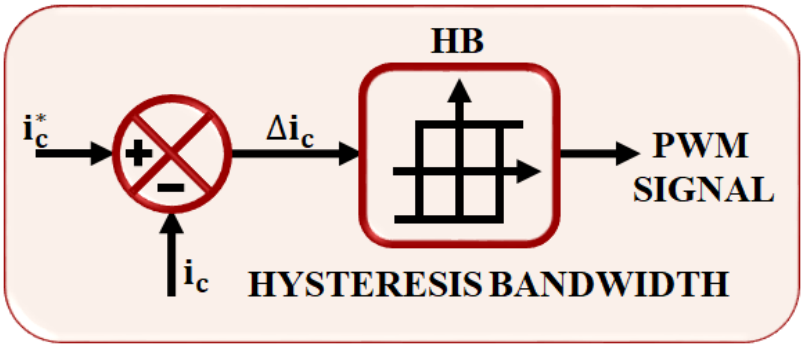

Fig. 4. Hysteresis Current Control.

compromise between these factors. This corrective output is then sent to the PWM generator, which is used to modulate the MMC's switching actions and control the current flow precisely.

3- 4- Generation of Reference Current by DQ Theory

In the proposed work, MMC integrated with DFIG-WECS, generating a reference current using dq theory. This enables the decoupling of active and reactive power control, essential for managing power quality and system stability.

The voltage and current from a 3φ The system is converted into a stationary reference frame $\alpha\beta$ using Clarke's transformation.

$$\begin{bmatrix} x_\alpha \\ x_\beta \end{bmatrix} = \begin{bmatrix} 1 & -1/2 & -1/2 \\ 0 & \sqrt{3}/2 & -\sqrt{3}/2 \end{bmatrix} \begin{bmatrix} x_a \\ x_b \\ x_c \end{bmatrix} \tag{8}$$

Where x defines voltage or current. Next Park's transformation is applied for transforming these signals into dq reference frame.

$$\begin{bmatrix} x_d \\ x_q \end{bmatrix} = \begin{bmatrix} sin\omega t & -cos\omega t \\ cos\omega t & sin\omega t \end{bmatrix} \begin{bmatrix} x_\alpha \\ x_\beta \end{bmatrix} \tag{9}$$

Where ωt specifies the angle of rotation, and this transformation results in DC components for a balanced, sinusoidal system. For converting the system again into $\alpha\beta$ frame into dq frame, the following expression is used

$$\begin{bmatrix} x_\alpha^* \\ x_\beta^* \end{bmatrix} = \begin{bmatrix} sin\omega t & cos\omega t \\ -cos\omega t & sin\omega t \end{bmatrix} \begin{bmatrix} x_d \\ x_q \end{bmatrix} \tag{10}$$

At last the signals are converted back into their original 3φ system as given by the expression

$$\begin{bmatrix} x_a^* \\ x_b^* \\ x_c^* \end{bmatrix} = \begin{bmatrix} 1 & 0 \\ -1/2 & \sqrt{3}/2 \\ -1/2 & -\sqrt{3}/2 \end{bmatrix} \begin{bmatrix} x_\alpha^* \\ x_\beta^* \end{bmatrix} \tag{11}$$

This conversion allows the control system to inject the optimal compensating current back into the system. Thereby, accurate current compensation takes place, even when the supply voltage is distorted or unbalanced.

4- Results and Discussion

Table 2 details the specification of the proposed work. Moreover, the detailed results of simulations, illustrating the performance of the proposed system in effectively controlling power flow, maintaining voltage and current quality, and enhancing the switch to balance efficiency is also discussed. In the system modeling, the WECS is designed using a DFIG coupled with a 5-level MMC, simulated in MATLAB/ Simulink. The DFIG parameters include a nominal power rating of 10 kW, frequency of 50 Hz, and detailed machine constants such as stator and rotor resistances, inductances, magnetizing inductance, inertia constant, and friction factor to ensure realistic dynamic behavior. The MMC converter is configured with an input voltage of 600 V, sub-module capacitance of 10 mF, and a switching frequency of 10 Hz to generate a high-quality multilevel output waveform. Simulation scenarios include variations in wind speed, which directly affect turbine torque, rotor speed, and pitch angle of the DFIG, allowing assessment of system response under fluctuating input conditions. Performance is evaluated in terms of output voltage and current waveforms, harmonic distortion, voltage stability, and current regulation.

The waveform in Fig. 5 demonstrates the performance of the DFIG system in a wind energy setup, highlighting critical parameters over time. The wind speed waveform shows a step change in wind speed occurring at 0.3s, indicating a variation in input wind conditions. This change impacts the turbine's performance. The turbine torque reacts to wind speed variations by exhibiting a dynamic decline, stabilizing after

Table 2. Design Component Parameter.

Parameter	Ratings
DFIG	
Pairs of Poles	3
Friction Factor	0.01F(pu)
No. of Turbines	4
Inertia Constant	0.685Hs
Magnetizing Inductance	2.9mH
Rotor Inductance	0.16mH(pu)
Rotor Resistance	0.016 Ω (pu)
Stator Resistance	0.023 Ω (pu)
Stator Inductance	0.18mH (pu)
Nominal Power	10kW
Frequency	50Hz
MMC converter	
Input voltage	600v
Frequency	50Hz
Capacitance voltage per sub module	10mF
Switching frequency	10 Hz

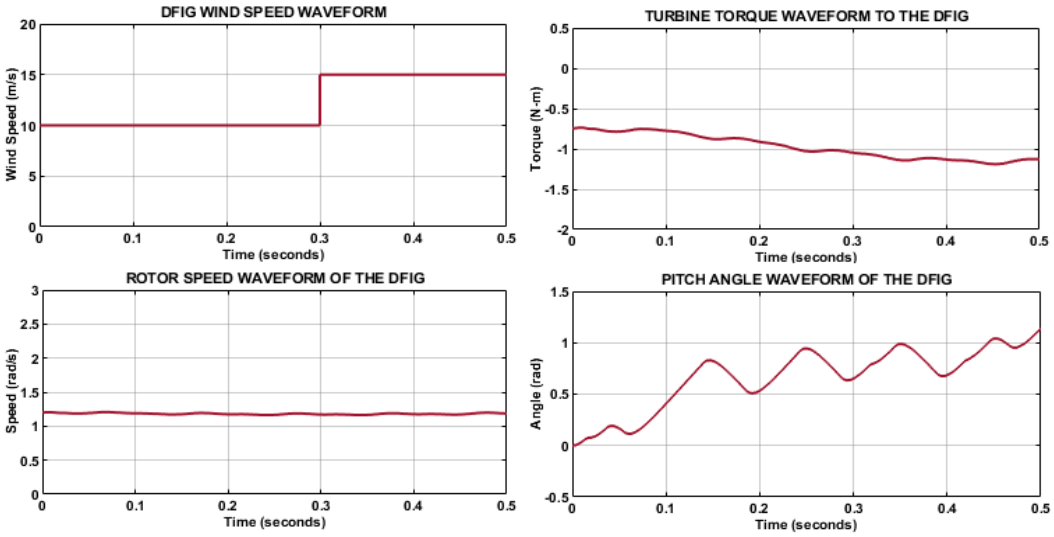

Fig. 5. Dynamic Response of DFIG in Wind System.

fluctuations at the initial stage. The rotor speed waveform of DFIG adjusts to maintain stability despite changes in input torque and wind speed. Finally, the pitch angle waveform shows dynamic increases and oscillations to regular output power and ensures system stability under varying wind speeds.

The output characteristics of the DFIG system are illustrated in Fig. 6. It is seen that the DFIG output voltage waveform fluctuates sinusoidally, indicating the generation of AC voltage, with variations in amplitude owing to system dynamics. The DFIG output current waveform exhibits sinusoidal characteristics, but with stable amplitude, representing steady delivery of current under controlled operation.

The voltage characteristics of the high frequency and low frequency converter is illustrated in Fig. 7. IT is seen from the high frequency converter waveform that rapid switching characteristics with a steady voltage level of 600V

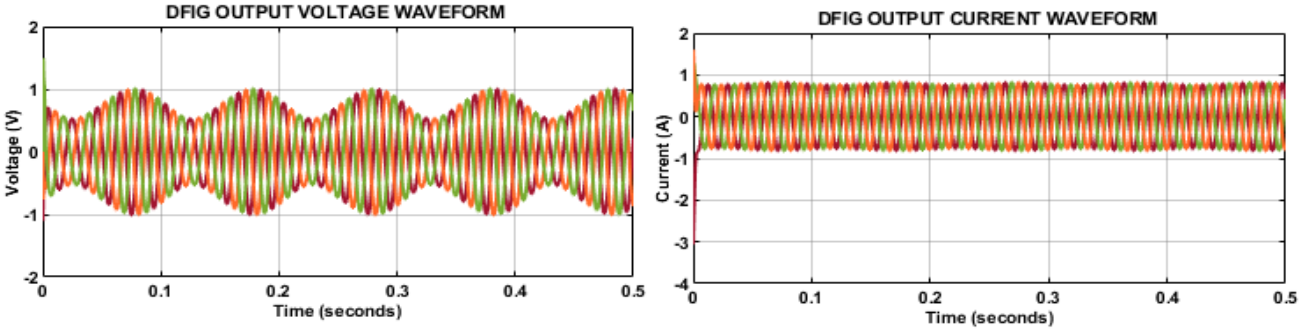

Fig. 6. Voltage and Current Output of DFIG System.

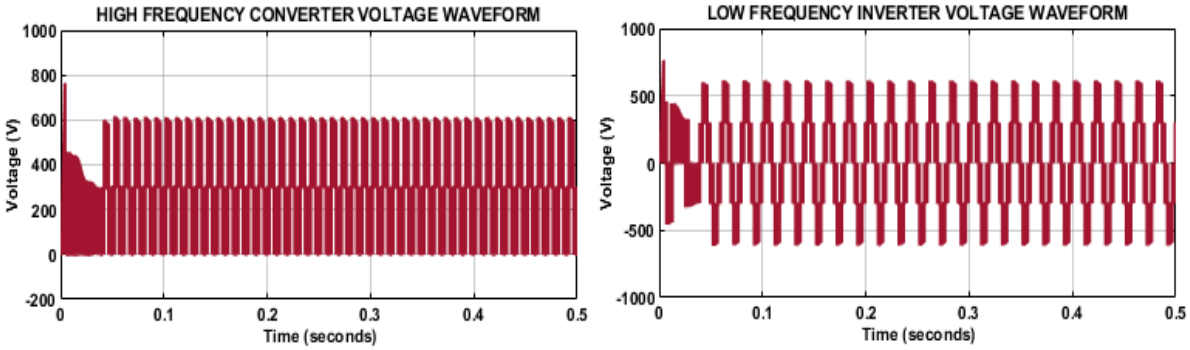

Fig. 7. Five-Level MMC Waveform.

are accomplished after initial oscillations. Whereas the low-frequency converter exhibits the same sinusoidal output with variations at the initial level, after continuing at 600V, representing the low-frequency voltage conversion essential for interfacing with the grid.

This waveform in Fig. 8 depicts the voltage and current characteristics of the three-phase inverter utilized in the proposed DFIG-based wind energy system. The three-phase inverter voltage waveform demonstrates sinusoidal voltages for each phase with a stable amplitude, ensuring effective power delivery to the load. The current waveform initially exhibits a transient response followed by steady sinusoidal currents for each phase, demonstrating the inverter's capability to stabilize and synchronize current output with the system.

The voltage and current waveforms observed at the grid interface in the proposed DFIG-based wind energy system are illustrated in Fig. 9. The grid voltage waveform represents consistent amplitude and frequency, indicating proper synchronization with grid standards. Whereas the grid current waveform initially shows variations, the three-phase sinusoidal voltage of 330V with before settling at 50A into steady sinusoidal currents for each phase.

The real and reactive power characteristics of the proposed DFIG-based wind energy system is demonstrated in Fig. 10. The real power waveform, which starts with an initial transient response and quickly stabilizes to deliver steady positive real power, reflecting effective energy transfer to the grid. The reactive power waveform, beginning with a negative transient before settling near zero, indicating successful reactive power compensation and improved power factor control. Fig. 11 showcases the THD waveform, which is at 1.35%, referring to minimized harmonic distortions. The harmonic spectrum illustrates that the proposed system successfully maintains the fundamental component at 50 Hz with a magnitude of 8.51, while suppressing most higher-order harmonics to negligible levels, yielding a very low THD of 1.35%. The small residual harmonics observed at multiples of the fundamental frequency are well within acceptable IEEE 519 standards, ensuring minimal waveform distortion. This low distortion level directly generates smoother voltage and current waveforms, leading to reduced losses in converters, transformers, and transmission lines. Furthermore, the reduced harmonic stress enhances the longevity of connected

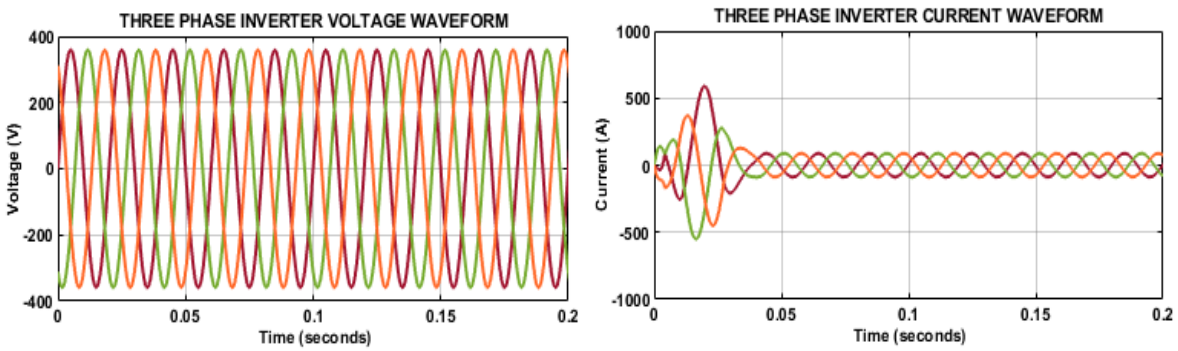

Fig. 8. Inverter Characteristics Waveform.

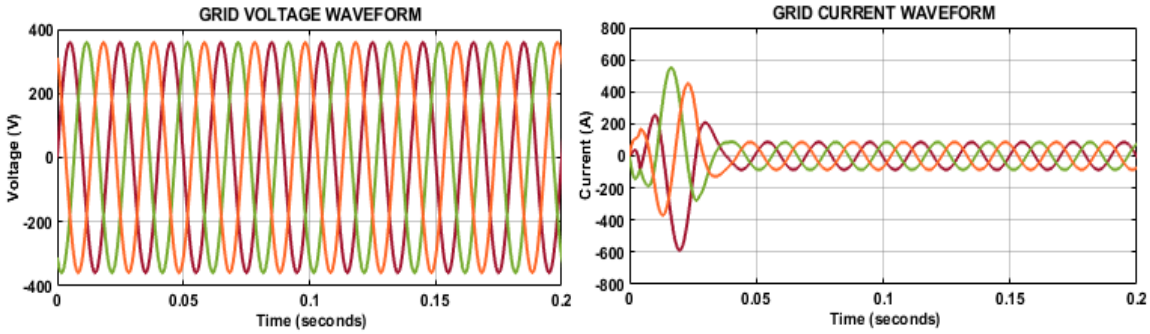

Fig. 9. Grid voltage and Current Waveform.

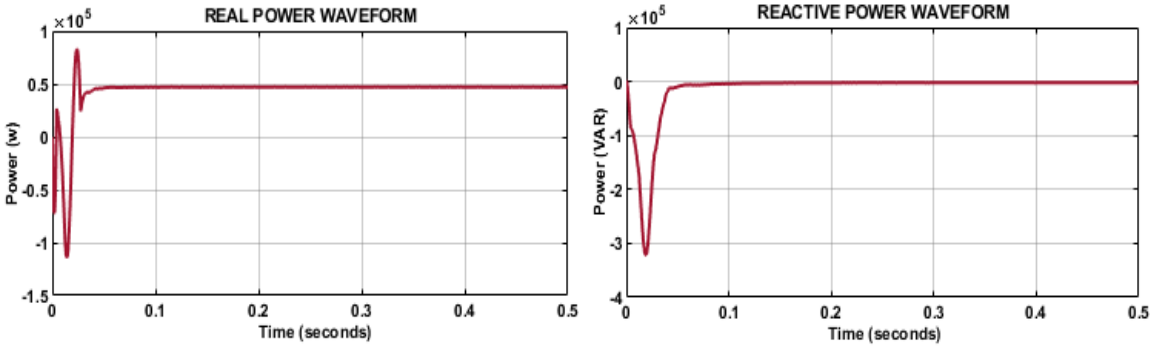

Fig. 10. Real and Reactive Power Waveform.

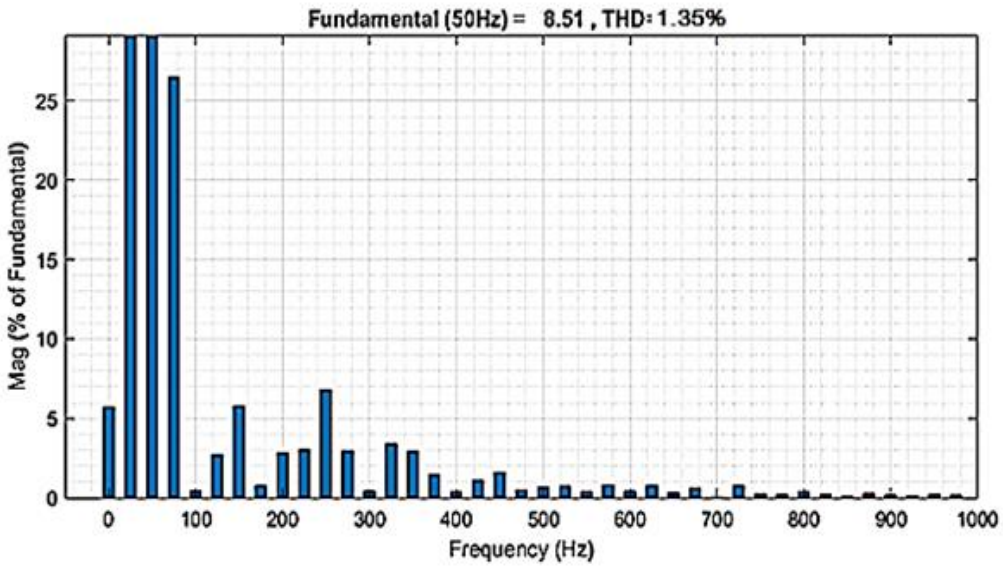

Fig. 11. THD Waveform.

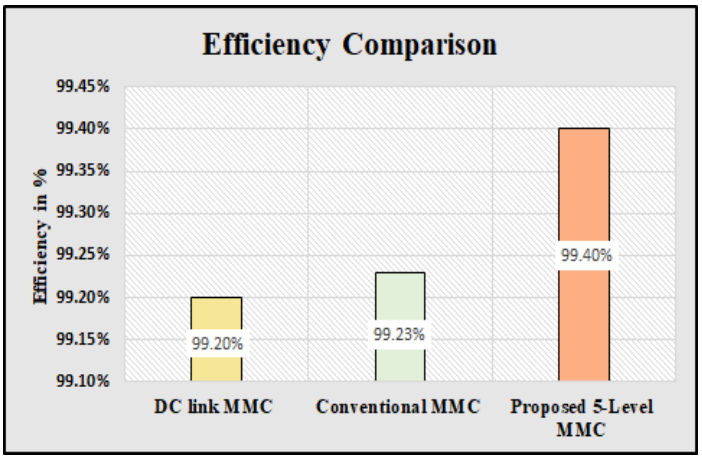

Fig. 12. Efficiency Comparison.

equipment, prevents overheating, and ensures stable grid synchronization. Overall, the precise THD reduction confirms that the system achieves high-quality power output, making it highly reliable for grid-connected wind energy applications.

Fig. 12 represents the efficiency comparison to analyze the performance efficacy of the 5-level MMC with various conventional converters. From the above chart, it is understandable that the 5-level MMC attained quite a higher efficiency of 99.40%, when compared to DC link MMC [18] and conventional MMC [19] that obtained 99.2% and 99.23% respectively, indicating enhanced converter performance is attained using 5-Level MMC within the proposed model.

The THD comparison graph is shown in Fig. 13, in which THD attained by EMMC [20] and conventional MMC [21] is compared with the proposed 5-Level MMC, and from the comparative evaluation, it is notable that the proposed MMC showcases reduced THD of 1.35% than [20] and [21], which obtained slightly higher THD of 1.7% and 1.41 %, referring to the presence of moderate or little harmonic distortions.

Fig. 14 demonstrates comparison of ripples attained by the proposed converter with [20] and [21], The above chart showcases that, ripple produced by the 5-Level MMC is 8, while the ripple produced by [20] and [21] is comparatively higher, indicating fluctuations, due to this reason the output power quality is also minimized. Therefore, utilization of 5-level MMC produces reduced ripples, hence ensuring

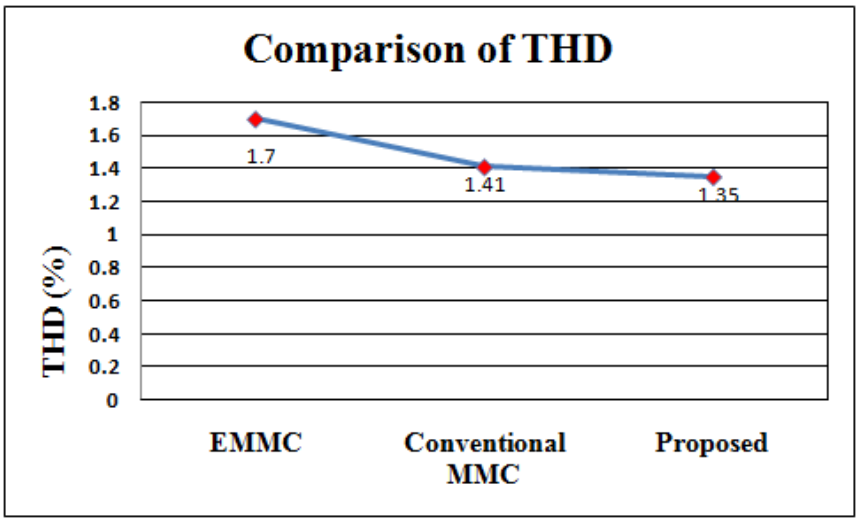

Fig. 13. THD Comparison.

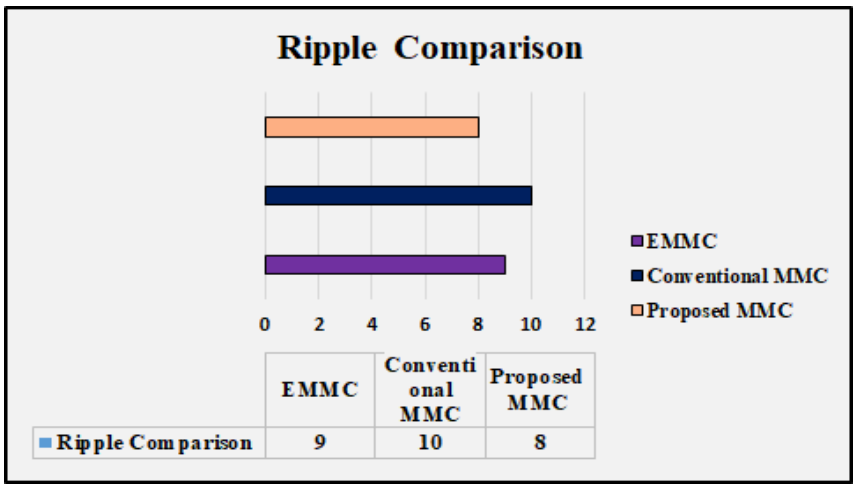

Fig. 14. Ripple Comparison.

reduced fluctuations with increased output power quality.

Table 3 presents a comparative analysis of THD achieved by the proposed system against several existing methods. The results clearly highlight that the proposed control strategy achieves the lowest THD of 1.35%, which is an improvement over other works. This marginal yet significant reduction in THD reflects the effectiveness of combining MMC topology, D-Q theory, and hysteresis control, ensuring enhanced power quality and stable grid integration. The results demonstrate that the proposed system not only competes with but outperforms state-of-the-art approaches, establishing its efficiency in mitigating harmonics and ensuring high-quality power delivery.

5- Conclusion

This paper presents a novel solution for enhancing the power quality challenges that are raised due to load fluctuations, voltage instability, and harmonic distortions by integrating a 5-Level MMC with DFIG-based WECS. The incorporation of the proposed converter in DFIG effectively improves the power quality by reducing harmonics, thus improving the voltage stability. In addition to this, the deployment of D-Q theory and HCC achieves optimum control, assuring smooth and consistent power supply to the grid. Furthermore, the utilization of an LC filter effectively removes any unwanted interferences, hence attaining sinusoidal waveforms with limited distortions. The proposed

Table 3. THD comparison with existing methods.

Methods	THD (%)
Kumar et al. [22]	7.89
Ramirez et al. [23]	1.71
Zheng et al. [24]	5.5
Jin et al. [25]	2.46
Jiang et al. [26]	1.36
Proposed	1.35

system's efficacy is validated through MATLAB/Simulink, which depicts that the proposed model minimizes THD of 1.35%, ensuring efficient and reliable power supply, with improved output power quality. Overall, the system assures a highly stable and effective power supply with reduced fluctuations, consequently increasing the power electronic technology for RES. However, the simulation-based validation, though effective, may not fully capture real-world uncertainties such as grid disturbances, parameter variations, or non-ideal switching behavior, which can impact system reliability. Future research can focus on developing real-time hardware-in-the-loop (HIL) testing and experimental validation for bridging the gap between simulation and practical implementation.

References

[1] R. K. Beniwal, M. K. Saini, A. Nayyar, B. Qureshi, A. Aggarwal A, "A critical analysis of methodologies for detection and classification of power quality events in smart grid", IEEE Access, 2021, vol. 9, pp. 83507-83534.

[2] S. Das, B. Singh, "Enhanced control of DFIG-based wind energy conversion system under unbalanced grid voltages using mixed generalized integrator", IEEE Journal of Emerging and Selected Topics in Industrial Electronics, 2022, vol. 3, no. 2, pp. 308-320.

[3] D. Krishnan, G. Prakash, N. Vengadachalam, R. Amaleswari, K. Eswaramoorthy, "Simulation of Reduced Switch Multilevel Inverter with New Topology for Less THD", 2022 International Conference on Computer, Power and Communications (ICCPC), 2022, pp. 621-626.

[4] J. Rodriguez, R. Heydari, Z. Rafiee, H. A. Young, F. Flores-Bahamonde, M. Shahparasti, "Model-free predictive current control of a voltage source inverter", IEEE Access, 2020, vol. 8, pp. 211104-211114.

[5] J. L. Rodríguez-Amenedo, S. A. Gómez, M. Zubiaga, P. Izurza-Moreno, J. Arza, J.D. Fernández, "Grid-forming control of voltage source converters based on the virtual-flux orientation", IEEE Access, 2023, vol. 11, pp. 10254-10274.

[6] L. Liu, Z. Zhang, Y. Yin, Y. Li, H. Xie, M. Zhang, Y. Zhao, R. Kennel, "A robust high-quality current control with fast convergence for three-level NPC converters in microenergy systems", IEEE Transactions on Industrial Informatics, 2023, vol. 19, no. 11, pp. 10716-10726.

[7] E. Akbari, A. Z. G. Seyyedi, "Power quality enhancement of distribution grid using a photovoltaic-based hybrid active power filter with three-level converter", Energy Reports, 2023, vol. 9, pp. 5432-5448.

[8] M. Humayun, M.M. Khan, A. Muhammad, J. Xu, W. Zhang, "Evaluation of symmetric flying capacitor multilevel inverter for grid-connected application", International Journal of Electrical Power & Energy Systems, 2020, vol. 115, pp. 105430.

[9] E. Candan, N. C. Brooks, A. Stillwell, R.A. Abramson, J. Strydom, R. C. Pilawa-Podgurski, "A six-level flying capacitor multilevel converter for single-phase buck-type power factor correction" IEEE Transactions on Power Electronics, 2021, vol. 37, no. 6, pp. 6335-6348.

[10] A. Lashab, D. Sera, T. Kerekes, Y. Terriche, A. Bouzid, J. C. Vasquez, J. M. Guerrero, "A cascaded H-bridge with integrated boosting circuit", IEEE Transactions on Power Electronics, 2020, vol. 36, no. 1, pp. 18-22.

[11] M. Sadoughi, A. Pourdadashnia, M. Farhadi-Kangarlu, S. Galvani, "PSO-optimized SHE-PWM technique in a cascaded H-bridge multilevel inverter for variable output voltage applications", IEEE Transactions on Power Electronics, 2022, vol. 37, no. 7, pp. 8065-8075.

[12] M. Sandhu, T. Thakur, "Modified cascaded H-bridge multilevel inverter for hybrid renewable energy applications", IETE Journal of Research, 2022, vol. 68, no. 6, pp. 3971-3983.

[13] S. D. S. Bettoni, H. D. O. Ramos, F. F. Matos, V. F. Mendes, "Cascaded h-bridge multilevel converter applied to a wind energy conversion system with open-end winding", Wind, 2023, vol. 3, no. 2, pp. 232-252.

[14] R. Yang, G. Shi, C. Zhang, G. Li, X. Cai, "Internal energy based grid-forming control for MMC-HVDC systems with wind farm integration", IEEE Transactions on Industry Applications, 2022, vol. 59, no. 1, pp. 503-512.

[15] A. Imam, R. Sreerama Kumar, Y. A. Al-Turki, "Modeling and simulation of a PI controlled shunt active power filter for power quality enhancement based on PQ theory", Electronics, 2020, vol. 9, no. 4, pp. 637.

[16] M. S. Priyadarshini, D. Krishna, K. V. Kumar, K. Amaresh, B. S. Goud, M. Bajaj, T. Altameem, W. El-Shafai, M. M. Fouda, "Significance of harmonic filters by computation of short-time Fourier transform-based time–frequency representation of supply voltage", Energies, 2023, vol. 16, no. 5, pp. 2194.

[17] M. Kashif, M. J. Hossain, E. Fernandez, S. Taghizadeh, V. Sharma, S. N. Ali, U. B. Irshad, "A fast time-domain current harmonic extraction algorithm for power quality improvement using three-phase Active power filter", IEEE Access, 2020, vol. 8, pp. 103539-103549.

[18] A. Shekhar, T. B. Soeiro, Y. Wu, P. Bauer, "Optimal Power Flow Control in Parallel Operating AC and DC Distribution Links", IEEE Transactions on Industrial Electronics, 2021, vol. 68, no. 2, pp. 1695-1706.

[19] F. Muhammad, H. Rasheed, "Power loss distribution and characterization of modular multilevel converter for smart grid applications", International Journal of Renewable Energy Research (IJRER), 2022, vol. 12, no. 3, pp. 1540-1551.

[20] D. Vozikis, F. Alsokhiry, G. P. Adam, Y. Al-Turki, "Novel enhanced modular multilevel converter for high-voltage direct current transmission systems", Energies, 2020, vol. 13, no. 9, pp. 2257.

[21] C. Huang, Y. Tian, J. Chen, "Circulating Current Suppression Combined with APF Current Control for the Suppression of MMC Voltage Fluctuations", Electronics, 2025, vol. 14, no. 1, pp. 64.

[22] A. R. Kumar, M. S. Bhaskar, U. Subramaniam, D. Almakhles, S. Padmanaban, J. Bo-Holm Nielsen, "An improved harmonics mitigation scheme for a modular multilevel converter," IEEE Access, 2019, vol. 7, pp. 147244-147255.

[23] D. Ramirez, M. E. Zarei, M. Gupta, J. Serrano, "Fast model-based predictive control (FMPC) for grid-connected modular multilevel converters (MMC)," International Journal of Electrical Power & Energy Systems, 2020, vol. 119, pp. 105951.

[24] G. Zheng, Y. Chen, Y. Kang, "A modular multilevel converter (MMC) based solid-state transformer (SST) topology with simplified energy conversion process and magnetic integration," IEEE Transactions on Industrial Electronics, 2020, vol. 68, no. 9, pp. 7725-7735.

[25] Y. Jin, Z. Zhang, Y. Huang, Z. Xu, F. Xu, "Harmonic filtering and fault ride-through of diode rectifier unit and modular multilevel converter based offshore wind power integration," IET Renewable Power Generation, 2023.

[26] Y. Jiang, H. Shu, M. Liao, "Fault-tolerant control strategy for sub-modules open-circuit fault of modular multilevel converter," Electronics, 2023, vol. 12, no. 5, pp. 1080.

HOW TO CITE THIS ARTICLE

K. Gowthami, D. Ravi Kishore, I. Sai Deepthi, K. Durga Prasad, G. Satish Kumar, Efficient Control and Five-Level MMC Integration for Power Quality Improvement in DFIG-Based Wind Energy System, AUT J. Elec. Eng., 58(1) (2026) 45-58.

DOI: 10.22060/eej.2025.24305.5677